One step route to the fabrication of arrays of TiO_2 nanobowls *via* a complementary block copolymer templating and sol–gel process†

Xue Li,[a] Juan Peng,[b] Joo-Hee Kang,[d] Jin-Ho Choy,[d] Martin Steinhart,[c] Wolfgang Knoll*[b] and Dong Ha Kim*[d]

Received 7th August 2007, Accepted 21st November 2007
First published as an Advance Article on the web 20th December 2007
DOI: 10.1039/b712125c

Highly dense, ordered arrays of a titania (TiO_2) nanomaterial with a bowl-shape morphology are generated by using poly(styrene-block-ethylene oxide) (PS-b-PEO) block copolymers as templates combined with a sol–gel process. Porous organic–inorganic hybrid films with titania nanodomains incorporated in the PEO domains can be produced by one step spin-coating. By manipulating the relative composition of the precursor ingredients, a simple protocol to fabricate hexagonally packed arrays of nanobowls is defined. Addition of a second inorganic precursor into the common solution leads to arrays of composite Au–TiO_2 nanobowls. Such organic–inorganic hybrids and pure titania nanostructures with controlled shape and size exhibit unique photophysical properties.

Introduction

Semiconductor or metal–semiconductor systems with low dimensional nanostructures such as nanowires, nanotubes, nanorings, nanobowls and nanobelts are extremely attractive due to their novel optical, electronic, magnetic and chemical properties.[1–3] It is well known that the properties of such nanostructured materials depend strongly on the size, shape, and composition.[2] Control over the structural parameters is one of the most challenging issues in developing new applications of nanostructured materials.[3] Many approaches for the preparation of nanostructured materials with controlled shape and dimensions have been reported. Selected examples include ring-like nanostructures *via* electron-beam lithography,[4] nanosphere templates,[5] porous templates,[6] or self-assembled amphiphilic triblock copolymer templates.[7]

TiO_2 is one of the most important oxide materials due to its wide range of applications.[8] Among these applications, TiO_2 has been used as an excellent photocatalyst and is a core constituent in solar-energy conversion devices.[9] In this regard, recent efforts have focused on the fabrication of TiO_2 nanostructures, such as nanoparticles,[10] nanowires,[11] nanotubes,[12] mesoporous materials, *etc.*[13] Ordered arrays of nanostructured TiO_2 nanobowls have also been fabricated using a self-assembled monolayer of PS spheres as a template.[14] Although the various nanostructured TiO_2 materials mentioned above have been suggested, it still remains a significant challenge to develop facile and effective methods for creating novel TiO_2 nanostructures with unprecedented properties.

Among numerous bottom-up strategies for nanofabrication, self-assembly of block copolymers (BCPs) has been recognized as versatile platform by which highly ordered periodic metallic, inorganic, and semiconductor nanostructures, such as nanodots,[15,16] 2-dimensional (2D) porous titania, and highly ordered 3D-networks[17–19] can be developed. In addition to typical classic morphologies (*e.g.*, lamellae, spheres, cylinders, and bicontinuous networks), recent experimental reports also show that other intricate morphologies, such as helices,[20] cylindrical networks,[21] nanotubes,[22] hollow hoops,[23] bowl-shaped micelles, and ring-like supramolecular assemblies can be observed from BCP solutions in selective solvents.[24] Such micellar solutions with non-classical morphologies may be utilized as templates to generate hybrid nanostructures with exquisite morphologies.

Combing micellar solutions with sol–gel chemistry, herein we suggest a rapid, simple fabrication protocol to synthesize nanoporous hybrid films and arrays of titania nanostructures with an unprecedented morphology, the so called nanobowl-shape. The methodology is based on an extension of our previous work where arrays of titania nanoparticles with controlled lateral spacing are prepared by one pot spin-coating of a common solution containing a BCP and an inorganic precursor onto a solid substrate.[25] The morphologies of the hybrid materials *via* a sol–gel process depend strongly on the type of template, composition, concentration, pH, solvent, *etc*.[26] Here, we demonstrate that the morphology can be efficiently controlled by manipulating the relative composition of the precursor solution. The resulting porous hybrid block copolymer–titania films show greatly enhanced room-temperature photoluminescence emission properties.

Experimental section

Materials

A PS-b-PEO diblock copolymer with a polydispersity index of 1.05 was purchased from Polymer Source, Inc. The number

[a]*School of Chemistry and Chemical Engineering, University of Jinan, 106 Jiwei Road, Jinan 250022, People's Republic of China*
[b]*Max Planck Institute for Polymer Research, Ackermannweg 10, 55128 Mainz, Germany*
[c]*Max Planck Institute for Microstructure Physics, Weinberg 2, D-06120 Halle, Germany*
[d]*Division of Nano Sciences and Department of Chemistry, 11-1 Daehyun-Dong, Seodaemun-Gu, Seoul 120-750, Korea*

† Electronic supplementary information (ESI) available: XRD patterns for SEO–TiO_2 and SEO–$HAuCl_4$–TiO_2 films; XPS spectra of PS-b-PEO/SG and Au–TiO_2 nanobowls obtained from PS-b-PEO–$HAuCl_4$-SG flims; photocatalytic activity of a PS-b-PEO–Au–TiO_2 film. See DOI: 10.1039/b712125c

average molecular weights of PS and PEO blocks are 19 000 g mol^{-1} and 6 400 g mol^{-1}, respectively. Titanium tetra-isopropoxide (TTIP, 97%), and tetrachloroauric (III) acid ($HAuCl_4 \cdot xH_2O$, Mw = 333.79) were purchased from Aldrich and used as received. Analytical grade toluene, isopropanol and hydrochloric acid (HCl, 37%) were purchased from Riedel-deHaën.

Substrates

Silicon (Si) wafers with a native oxide layer (*ca.* 2.5 cm × 2.5 cm) were cleaned in piranha solution (70 : 30 v/v concentrated H_2SO_4 : H_2O_2. Caution! Piranha solution reacts violently with organic compounds and should not be stored in closed containers), thoroughly rinsed with Milli-Q water, and then blown dry with nitrogen gas.

Film preparation

PS-b-PEO and Au-loaded PS-b-PEO (molar ratio of $HAuCl_4$/EO was 0.1) solutions of 1.0 wt% in toluene were used in this study. The preparation process of the sol–gel (SG) precursor solutions was described previously.[27] The molar ratio of TTIP / HC l in the sol–gel precursor solution was adjusted from 2.0 to 0.5. The desired amount of sol-gel precursor solution was mixed with the PS-b-PEO solution or the Au-loaded PS-b-PEO solution and stirred for 30 min. The amount of precursor relative to the polymer (ϕ) was 15.0% v/v.

The hybrid inorganic–organic films were produced simply by spin-coating the mixture solution on a piece of Si substrate. The obtained films were dried under ambient conditions to induce crosslinking of the sol–gel precursor. In order to remove the block copolymer template and reduce $HAuCl_4$ to metallic Au, the films were treated with deep UV irradiation in air (λ = 254 nm) for 2 d.[28]

Characterization

AFM height and phase contrast images were obtained using a Digital Instruments Dimension 3100 scanning force microscope in tapping mode with an Olympus cantilever. Field emission scanning electron microscopy (FESEM) images were obtained with a LEO 1530 "Gemini". The average diameters of the pores were determined by the Image J program (NIH). High resolution transmission electron microscopy (HRTEM) and energy dispersive spectroscopy (EDS) measurements were carried out on a Tecnai F30 at 200 kV. The crystal structures of the nanostructured TiO_2 and Au were studied by powder X-ray diffraction (XRD) on a Rigaku D/MAX at 2200 V using Ni-filtered Cu Kα radiation with a graphite diffracted beam monochromator. XPS measurements were performed on a Perkin-Elmer-Physical Electronics 5100 with Mg Kα excitation (400 W). Spectra were obtained at a take-off angle of 15°. Photoluminescence (PL) spectra were measured using a SPEX FLUOROLOG II (212) instrument at an excitation wavelength of 260 nm. The hybrid films were treated at 90 °C for 1 h in a vacuum or with UV light for 2 d in air before PL measurements.

Results and discussion

In the present PS-b-PEO–sol-gel (SG) system, we found that the morphologies of the hybrid films depend significantly on the molar ratio of TTIP / HCl in the sol–gel precursor solution. When the molar ratio of TTIP / HCl in the precursor solution is 2.0, worm-like structures are formed. If the molar ratio of TTIP / HCl in the precursor solution is changed to 0.5, porous hybrid films are obtained. Fig. 1 shows the FESEM images of the hybrid PS-*b*-PEO/SG films spin-coated on silicon substrates at 2500 rpm. Fig. 1A shows that the PEO–titania film exhibits worm-like structures while an array of circular pores is shown in Fig. 1B. The average diameter of the pores (D) is measured to be about 60 nm. The perspective view shown in Fig. 1C illustrates that the pores do not span through the entire film. Similar porous morphologies are observed if additives, such as $HAuCl_4$, are introduced to the system (data not shown). We have already utilized the same PS-b-PEO/sol–gel system to generate TiO_2 nanoparticle arrays.[25,27] The difference between the previous system and the present one lies in the relative

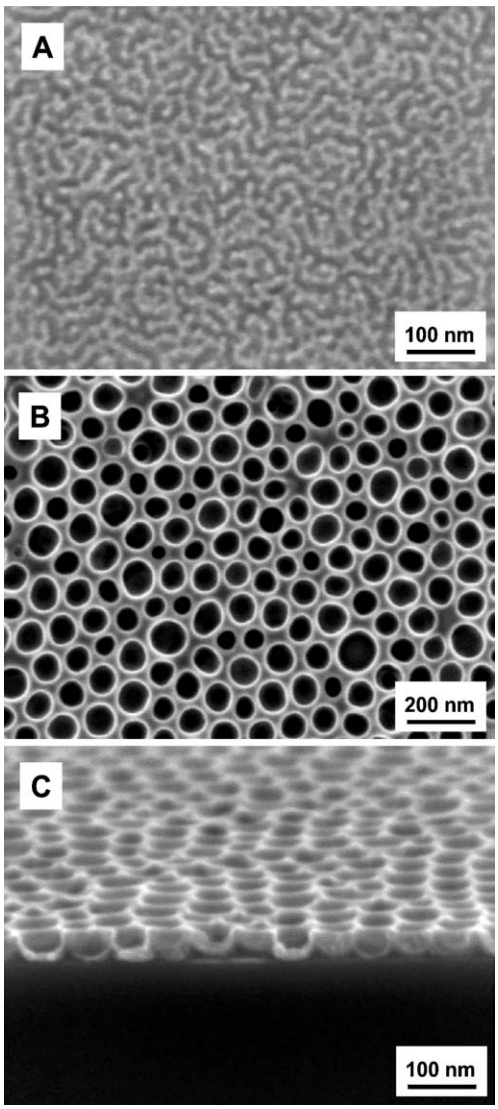

Fig. 1 FESEM images of the hybrid films of PS-b-PEO/SG15 with worm-like structures (A) and porous structures (B); (C) is the perspective view of the porous hybrid film. The molar ratio of TTIP : HCl is 2.0 in (A) and 0.5 in (B) and (C).

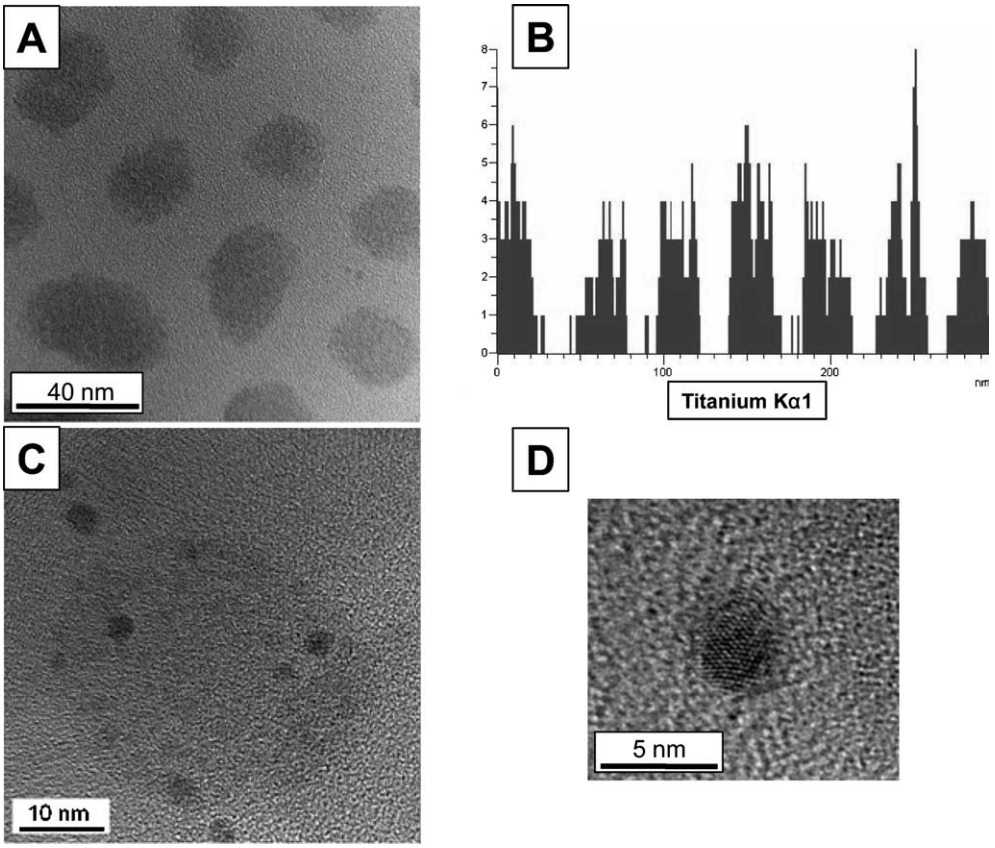

Fig. 2 HRTEM image (A) and its EDS (B) spectrum of the hybrid film of PS-b-PEO/SG15 with porous structures. HRTEM image of the hybrid film of PS-b-PEO–$HAuCl_4$/SG15 (C) and that of an Au domain.

amount of HCl solution. Therefore it is believed that the HCl solution has a critical role on the morphology of the hybrid film.[29]

To investigate the structures of the hybrid films, HRTEM and EDS measurements were performed on both PS-b-PEO/SG and PS-b-PEO-$HAuCl_4$/SG films. Darker titania nanodomain arrays in the PS matrix are observed in the TEM image of the PS-b-PEO/SG film (Fig. 2A) and the periodic nature of the titania moiety is clearly evidenced in the EDS spectrum (Fig. 2A). If $HAuCl_4$ is added to the system, most of it forms nanoparticles which are sporadically dispersed inside the titania domains (Fig. 2C). A further magnified HRTEM image of an Au nanoparticle domain reveals clear lattice fringes of the crystalline structure as shown in Fig. 2D

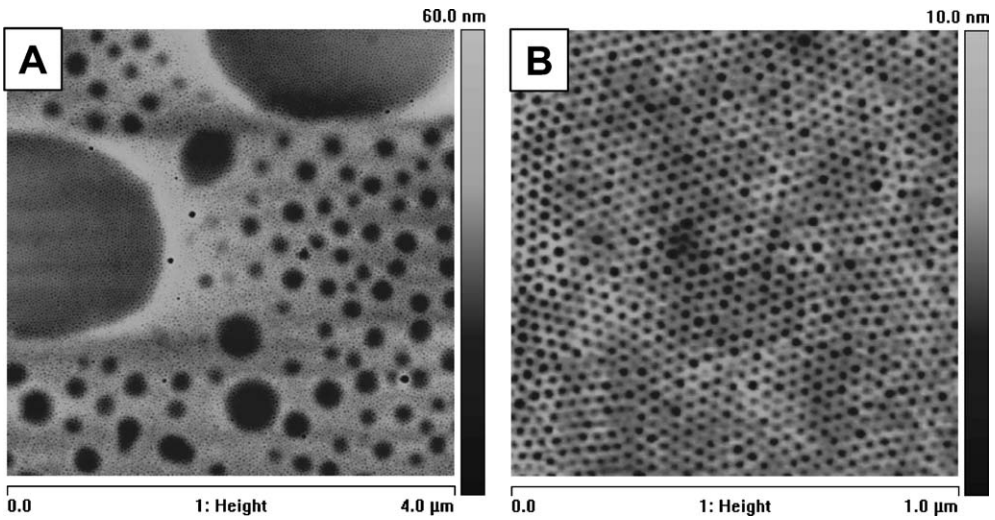

Fig. 3 AFM height images of the surfaces of the reference PS–b–PEO films prepared following the same procedure as for the hybrid samples except for the addition of TTIP; (A) in low magnification (4 μm × 4 μm); (B) in high magnification (1 μm × 1 μm).

In order to explain the formation of the porous structures observed in Fig. 1B, the morphologies of the pure PS-b-PEO film (noted as the reference film) were prepared following the same procedure as for the hybrid samples, except for TTIP, and were analyzed. Fig. 3 displays the AFM images of the reference film. It is noted that the surfaces of the film shown in Fig. 3A have many large circular regions (darker parts) of different sizes. These darker regions are lower in height than the other brighter regions of the film. However, the magnified AFM images of the PS-b-PEO reference film (Fig. 3B) show that the ordering of the cylindrical array is markedly enhanced compared with that of the film spin-coated directly from the PS-b-PEO solution indicating that highly ordered arrays of nanoscopic, cylindrical domains of PEO are obtained at the surface of the reference film. The average diameter of the PEO cylinders is about 20 nm, which is much smaller than that of the hybrid film observed in Fig. 1B. These results reveal that the formation mechanism of the hybrid film is different from that of the reference film.

Two key processes, *i.e.*, the difference in solubility of the PEO and the PS blocks in the mixed solvents and the incorporation of titania oligomers into PEO microdomains, are believed to play an important role in the formation of the porous nanostructures. PS-b-PEO can form micelles in toluene. The titania sol–gel precursor is composed of TTIP, HCl (37%), toluene and isopropanol. If the sol–gel precursor is mixed with the PS-b-PEO

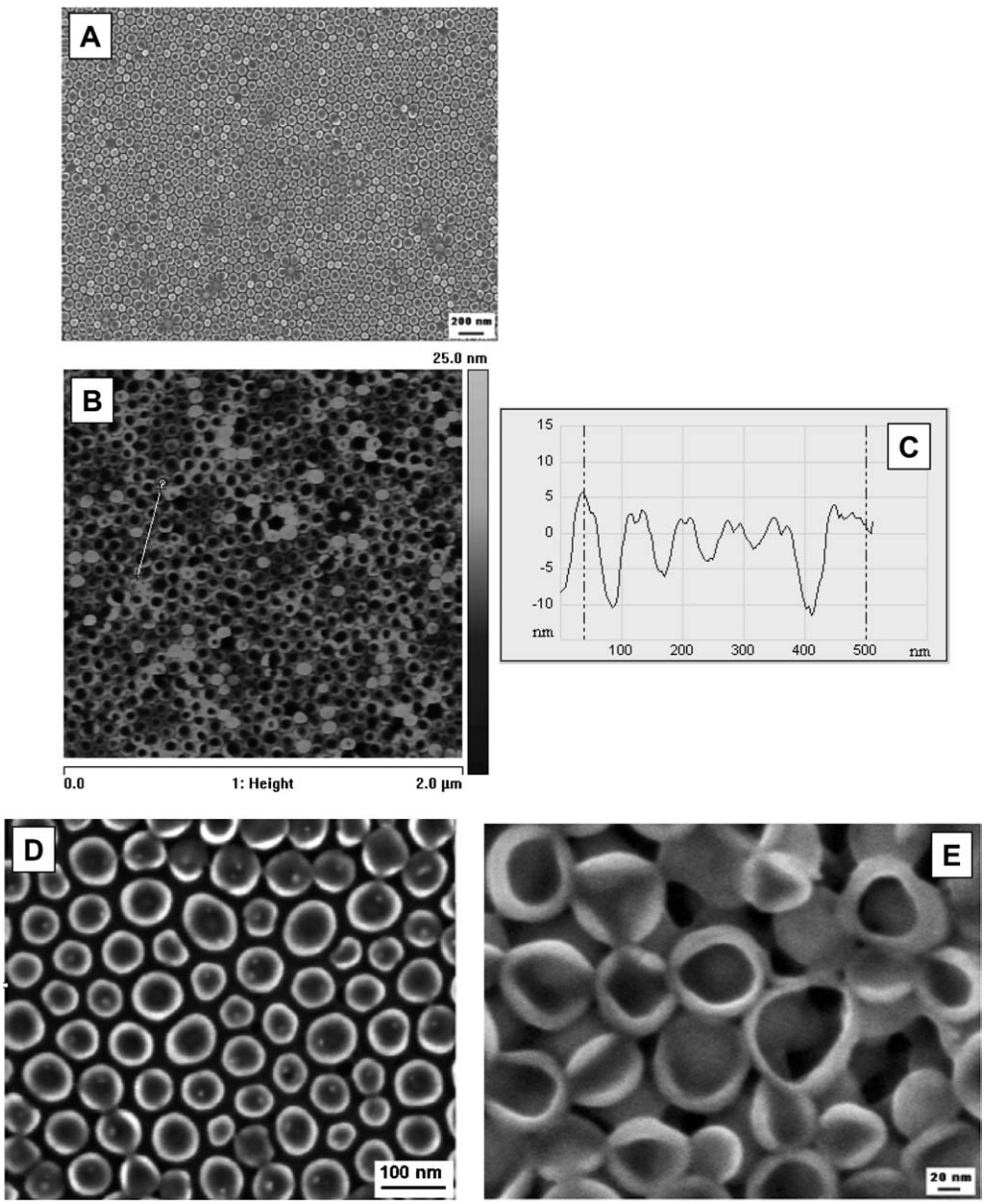

Fig. 4 FESEM image (A), AFM height image (B) of the arrays of TiO_2 nanobowls obtained from porous hybrid PS-b-PEO/SG15 films after removal of the block copolymers. (C) line scan taken along the line shown in (B). (D) FESEM image of Au–TiO_2 nanobowls obtained from porous hybrid PS-b-PEO–$HAuCl_4$/SG15 films after removal of the block copolymers. (E) FESEM image of the TiO_2 nanobowls arrays obtained from thicker initial hybrid PS-b-PEO/SG15 films after removal of the block copolymers.

solution or the Au-loaded PS-b-PEO solution, isopropanol, a small amount of water and titania oligomers will be segregated into the PEO domains due to their favorable interactions. This effect may cause the aggregation number of the block copolymer micelles to increase.[30] Provided that the titania oligomers are uniformly distributed in the PEO domains,[25] it is reasonable to deduce that the sizes of the hydrophilic PEO domains, which are surrounded by PS chains, will increase. That is, cooperative self-assembly of both PS-b-PEO copolymers and titania oligomers in the mixed solvents leads to large aggregates consisting of a soluble PS corona and a large core containing PEO chains, titania oligomers, isopropanol and water. In addition, the viscosity of the system will become larger than that of the reference system (no TTIP) due to the incorporation of titania nanostructures into PEO domains.[31]

Since the evaporation rates of organic solvents (toluene and isopropanol) are larger than that of water, preferential evaporation of the organic solvents during spin-coating will cause the relative content of water increase in the liquid film and induce a cooling of the solution surface. The viscosity of the liquid film increases and a gelation process of PS blocks along with a phase separation process will occur if the solvents evaporate further during spin-coating. In this process, the hydrophilic domains are encapsulated by PS blocks and their coalescence is prevented. Water is still retained and uniformly distributed in the PEO domains. Complicated surface currents (gas flow, convection, and Marangoni flows) induce compact arrays of aggregates composed of hydrophilic cores and outer PS blocks. After the evaporation of water from the polymer layer on the top of the film, a film with porous structures forms.[32] If the system does not contain TTIP, the hydrophilic PEO domains can partially coalesce during spin-coating due to lower viscosity and a film with lower and larger circular regions of different size is formed (Fig. 3A).

To induce arrays of pure TiO_2 nanostructures on the silicon substrates from the initial hybrid organic–inorganic films, the block copolymer templates were removed by exposure to deep UV irradiation. The FESEM image (Fig. 4A) reveals that isolated titania nanostructures form on the surface after removal of the block copolymer. The AFM height image and its line scan shown in Fig. 4B and C indicate that these nanostructures are bowl-like. With the addition of the $HAuCl_4$ precursor to the PS-b-PEO solution, an array of titania nanobowls containing smaller Au nanoparticles in each bowl are also obtained after removing the block copolymer (Fig. 4D). From thicker hybrid films prepared by spin-coating at 400 rpm, the same type of morphologies were observed after removing the block copolymer (Fig. 4E), indicating that the large aggregates are formed in the mixture solution of PS-b-PEO and the titania sol–gel precursor. Based on the mechanism discussed above, a schematic diagram of the formation process to generate TiO_2 nanobowls on silicon substrates is depicted in Fig. 5.

We performed an in-depth analysis of the crystallinity of the hybrid Au–TiO_2 nanodomains by XRD measurements. It was found that the initial PS-b-PEO–TiO_2 and PS-b-PEO–$HAuCl_4$–TiO_2 films did not exhibit any noticible peaks, indicating that the inorganic nanodomains in these films are amorphous (see Fig. S2, ESI†). The XRD patterns for the arrays of TiO_2 and Au–TiO_2 are obtained from calcination of the initial hybrid films

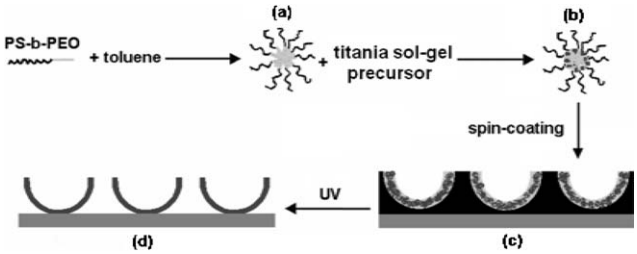

Fig. 5 Schematic illustration of the formation process to generate TiO_2 nanobowls on a silicon (Si) substrate. (a) Formation of a micellar solution of PS-b-PEO copolymers in toluene. (b) The micellar solution is mixed with the desired amount of sol–gel precursor solution; the titania precursor is selectively incorporated into the PEO domains. (c) Formation of nanoporous organic–inorganic hybrid films by spin-coating the mixture solution on a Si substrate. (d) Formation of arrays of TiO_2 nanobowls after the removal of the block copolymer matrix.

at 600 °C for 4 h under a N_2 atmosphere as shown in Fig. 6A and B, respectively. Characteric peaks of typical anatase TiO_2 are observed in Fig. 6A, consistent with our previous results,[25b] where the 2 θ (spacing) peaks can be assigned as 25.66 (3.47Å), 38.32 (2.35Å), 48.32 (1.88Å) and 54.96 (1.67Å), respectively. From the spectrum of Au–TiO_2 in Fig. 6B, crystalline Au structures are also evidenced by the additional peaks (denoted as circles) along with the same feature from the TiO_2, implying that the presence of Au did not alter the crystalline form of TiO_2 domains. Here, the two theta(spacing) is assigned as 25.78(3.45Å), 33.24(2.69Å), 38.54(2.33Å), 44.76(2.02Å), and 48.46(1.88Å). The chemical identity of the surfaces of the hybrid films was also investigated by XPS (see Fig. S2 in the ESI†).[33,34]

As a systematic approach to explore the photophysical properties in line with our previous works, the photoluminescence (PL) properties of the porous hybrid PS-b-PEO/SG films as well as the arrays of TiO_2 nanobowls were measured with an excitation wavelength of $\lambda = 260$ nm. Fig. 7 shows the representative PL spectra from a porous hybrid film and an array of TiO_2 nanobowls. It can be seen from Fig. 7A and B, that the initial hybrid sample exhibits strong PL with a main peak located at

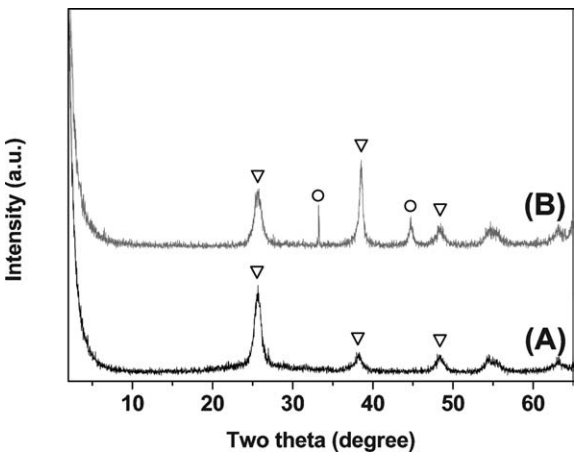

Fig. 6 XRD patterns for the arrays of TiO_2 (A) and Au–TiO_2 (B) obtained from calcination of the initial hybrid films at 600 °C for 4 h under a N_2 atmosphere. The triangles and circles represent characteristic peaks of the TiO_2 anatase phase and gold nanocrystals, respectively.

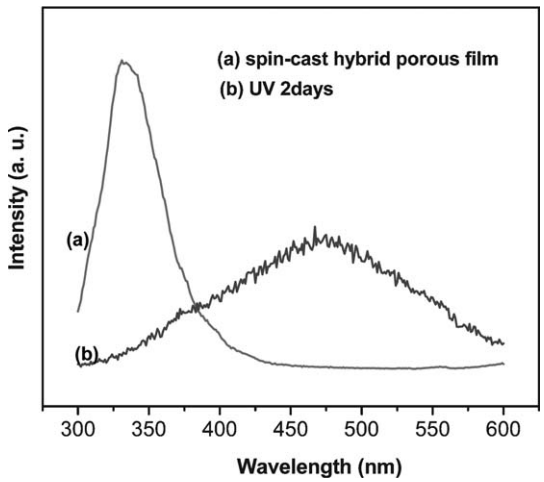

Fig. 7 (a) PL spectrum of a porous hybrid PS-b-PEO/SG film. (b) PL spectrum from arrays of TiO_2 nanobowls obtained after the removal of the PS-b-PEO template by deep UV irradiation. The excitation wavelength is 260 nm.

about $\lambda = 333$ nm upon photoexcitation at $\lambda = 260$ nm, which is close to the emission band of nanocrystals of TiO_2 and may be attributed to the band-edge luminescence at room-temperature.[35] However, the peak position is different from the PL spectra of the TiO_2 nanoparticles.[36] After the removal of the block copolymer matrix, the PL spectrum of the arrays of TiO_2 nanobowls exhibits a broad band with a main peak centered at about $\lambda =$ 473 nm upon photoexcitation at $\lambda = 260$ nm, which may be attributed to the oxygen vacancies.[37] We also investigated into the photocatalytic activity of a representative hybrid PS-b-PEO–$HAuCl_4$–TiO_2 film in terms of the decomposition of a dye (methylene blue) and found out that such a hybrid system exhibits comparable activity with similar nanostructured TiO_2 (see Fig. S3 in the ESI†).

Conclusions

We presented a simple method to generate nanoporous organic–inorganic hybrid films and arrays of TiO_2 or Au–TiO_2 nanobowls using PS-b-PEO block copolymers as templates in combination with a sol–gel process. Nanoporous hybrid films were obtained by spin-coating the mixture of the PS-b-PEO solution and the titania sol–gel precursors on solid substrates. Inclusion of other additives, such $HAuCl_4$, essentially did not alter the morphology of the porous hybrid films. The mechanism of structural evolution was explained by several factors including the selective incorporation of a titania precursor into the PEO domains, the change of self-organization behavior of PS-b-PEO, and complicated surface currents involved in the spin-coating process. By removing the block copolymer templates by deep UV irradiation or calcination, the arrays of TiO_2 or Au–TiO_2 nanobowls could be obtained on the substrate surface. The crystalline nature of the TiO_2 or Au–TiO_2 nanobowls was also analysed by HRTEM and XRD studies, revealing a typical anatase phase of TiO_2 nanodomains. Finally such hybrid films exhibited characteristic PL properties and photocatalytic activity.

Acknowledgements

This work was funded by the National Natural Science Foundation of China (20674030) and Shandong Natural Science Foundation (Y2006B02). D. H. Kim thanks for the support by the Seoul Research and Business Development Program (10816), and by the Korea Research Foundation Grant funded by the Korean Government (MOEHRD, Basic Research Promotion Fund) (KRF-2006-003-D00138). This work was financially supported by the SRC program of MOST/KOSEF through the Center for Intelligent Nano-Bio Materials at Ewha Womans University (grant: R11-2005-008-00000-0). M. Steinhart thanks the German Research Foundation (STE 1127/8-1) for funding.

References

1 (*a*) C. Burda, X. Chen, R. Narayanan and M. A. El-Sayed, *Chem. Rev.*, 2005, **105**, 1025–1102; (*b*) D. J. Milliron, S. M. Hughes, Y. Cui, L. Manna, J. B. Li, L. W. Wang and A. P. Alivisatos, *Nature*, 2004, **430**, 190–195; (*c*) T. Hyeon, *Chem. Commun.*, 2003, 927–934; (*d*) S. H. Sun, C. B. Murray, D. Weller, L. Folks and A. Moser, *Science*, 2000, **287**, 1989–1992.
2 (*a*) P. Moriarty, *Rep. Prog. Phys.*, 2001, **64**, 297–381; (*b*) C. B. Almquist and P. Biswas, *J. Catal.*, 2002, **212**, 145–156; (*c*) P. E. De Jongh and D. Vanmaekelbergh, *Phys. Rev. Lett.*, 1996, **77**, 3427–3430.
3 (*a*) M. Law, J. Goldberger and P. Yang, *Annu. Rev. Mater. Res.*, 2004, **34**, 83–122; (*b*) H. Terrones and M. Terrones, *New J. Phys.*, 2003, **5**, 126.
4 M. Kläui, C. A. F. Vaz, J. A. C. Blanda, W. Wernsdorfer, G. Faini, E. Cambril and L. J. Heyderman, *Appl. Phys. Lett.*, 2003, **83**, 105–107.
5 J. Aizpurua, P. Hanarp, D. S. Sutherland, M. Käll, G. W. Bryant and F. J. García de Abajo, *Phys. Rev. Lett.*, 2003, **90**, 057401–057404.
6 K. L. Hobbs, P. R. Larson, G. D. Lian, J. C. Keay and M. B. Johnson, *Nano Lett.*, 2004, **4**, 167–171.
7 J. Zhu and W. Jiang, *Mater. Chem. Phys.*, 2007, **101**, 56–62.
8 (*a*) A. Linsebigler, G. Lu and J. T. Yates, *Chem. Rev.*, 1995, **95**, 735–758; (*b*) M. Jakob, H. Levanon and P. V. Kamat, *Nano Lett.*, 2003, **3**, 353–358; (*c*) K. Naoi, Y. Ohko and T. Tatsuma, *J. Am. Chem. Soc.*, 2004, **126**, 3664–3668; (*d*) P. D. Cozzoli, R. Comparelli, E. Fanizza, M. L. Curri, A. Agostiano and D. Laub, *J. Am. Chem. Soc.*, 2004, **126**, 3868–3879.
9 G. Li, L. Li, J. Boerio-Goates and B. F. Woodfield, *J. Am. Chem. Soc.*, 2005, **127**, 8659–8666.
10 (*a*) S. Dohshi, M. Takeuchi and M. Anpo, *Catal. Today*, 2003, **85**, 199; (*b*) M. Niederberger, M. H. Bartl and G. D. Stucky, *Chem. Mater.*, 2002, **14**, 4364–4370.
11 (*a*) J. M. Wu, H. C. Shih, W. T. Wu, Y. K. Tseng and Y. C. Chen, *J. Cryst. Growth*, 2005, **281**, 384–390; (*b*) Y. Lei and L. D. Zhang, *J. Mater. Res.*, 2001, **16**(4), 1138–1144.
12 M. S. Sander, M. J. Gôté, W. Gu, B. M. Kile and G. P. Tripp, *Adv. Mater.*, 2004, **16**, 2052–2057; C. M. Ruan, M. Paulose, O. K. Varghese, G. K. Mor and C. A. Grimes, *J. Phys. Chem. B*, 2005, **109**(33), 15754–15759; G. K. Mor, O. K. Varghese, M. Paulose and C. A. Grimes, *Adv. Funct. Mater.*, 2005, **15**(8), 1291–1296.
13 H.-S. Yun, K. Miyazawa, H. S. Zhou, I. Honma and M. Kuwabara, *Adv. Mater.*, 2001, **13**, 1377–1380.
14 X. D. Wang, E. Graugnard, J. S. King, Z. L. Wang and C. J. Summers, *Nano Lett.*, 2004, **4**(11), 2223–2226.
15 (*a*) G. Kästle, H.-G. Boyen, F. Weigl, G. Lengl, T. Herzog, P. Ziemann, S. Riethmüller, O. Mayer, C. Hartmann, J. P. Spatz, M. Möller, M. Ozawa, F. Banhart, M. G. Garnier and P. Oelhafen, *Adv. Funct. Mater.*, 2003, **13**, 853; (*b*) J. P. Spatz, S. Mösser, C. Hartmann, M. Möller, T. Herzog, M. Krieger, H.-G. Boyen and P. Ziemann, *Langmuir*, 2000, **16**, 407.
16 S. Förster and T. Plantenberg, *Angew. Chem., Int. Ed.*, 2002, **41**, 688–714.
17 Y.-H. Cho, G. Cho and J.-S. Lee, *Adv. Mater.*, 2004, **16**, 1814–1817.
18 B. Smarsly, D. Grosso, T. Brezesinski, N. Pinna, C. Boissière, M. Antonietti and C. Sanchez, *Chem. Mater.*, 2004, **16**, 2948–2952.

19 D. Grosso, C. Boissière, B. Smarsly, T. Brezesinski, N. Pinna, P. A. Albouy, H. Amenitsch, M. Antonietti and C. Sanchez, *Nat. Mater.*, 2004, **3**, 787–792.
20 J. Cornelissen, M. Fischer, N. Sommerdijk and R. J. M. Nolte, *Science*, 1998, **280**, 1427–1430.
21 S. Jain and F. S. Bates, *Science*, 2003, **300**, 460–464.
22 (*a*) K. Yu, L. F. Zhang and A. Eisenberg, *Langmuir*, 1996, **12**, 5980–5984; (*b*) J. Raez, I. Manners and M. A. Winnik, *J. Am. Chem. Soc.*, 2002, **124**, 10381–10395.
23 L. F. Zhang, C. Bartels, Y. S. Yu, H. W. Shen and A. Eisenberg, *Phys. Rev. Lett.*, 1997, **79**, 5034–5037.
24 (*a*) I. C. Riegel, A. Eisenberg, C. L. Petzhold and D. Samios, *Langmuir*, 2002, **18**, 3358–3363; (*b*) D. J. Pochan, Z. Y. Chen, H. G. Cui, K. Hales, K. Qi and K. L. Wooley, *Science*, 2004, **306**, 94–97.
25 (*a*) D. H. Kim, Z. C. Sun, T. P. Russell, W. Knoll and J. S. Gutmann, *Adv. Funct. Mater.*, 2005, **15**, 1160–1164; (*b*) M. B. Raschke, L. Molina, T. Elsaesser, D. H. Kim, W. Knoll and K. Hinrichs, *ChemPhysChem*, 2005, **6**, 2197–2203.
26 (*a*) S. Förster and M. Antonietti, *Adv. Mater.*, 1998, **10**, 195–217; (*b*) G. Wanka, H. Hoffmann and W. Ulbricht, *Macromolecules*, 1994, **27**, 4145–4159.
27 Z. Sun and J. S. Gutmann, *Physica A*, 2004, **339**, 80–85.
28 (*a*) S. Haseloh, S. Y. Choi, M. Mamak, N. Coombs, S. Petrov, N. Chopra and G. A. Ozin, *Chem. Commun.*, 2004(13), 1460–1461; (*b*) J.-U. Kim, S.-H. Cha, K. Shin, J. Y. Jho and J.-C. Lee, *Adv. Mater.*, 2004, **16**, 459–464.
29 Y. J. Cheng and J. S. Gutmann, *J. Am. Chem. Soc.*, 2006, **128**, 4658–74.
30 L. J. M. Vagberg, K. A. Cogan and A. P. Gasto, *Macromolecules*, 1991, **24**, 1670–1677.
31 Q. Zhang and L. A. Archer, *Macromolecules*, 2004, **37**, 1928–1936.
32 O. Pitois and B. François, *Eur. Phys. J. B*, 1999, **8**, 225–231.
33 (*a*) J. M. McKay and V. E. Henrich, *Surf. Sci.*, 1984, **137**, 463–472; (*b*) R. Zimmermann, P. Steiner, R. Claessen, F. Reinert and S. Hufner, *J. Electron Spectrosc. Relat. Phenom.*, 1998, **96**, 179–186.
34 (*a*) M. Brust and M. Walker, *J. Chem. Soc., Chem. Commun.*, 1994(7), 801–802; (*b*) H. G. Boyen and G. Kästle, *Science*, 2002, **297**, 1533–1536; (*c*) K. Juodkazis, J. Juodkazyte, V. Jasulaitiene, A. Lukinskas and B. Sebeka, *Electrochem. Commun.*, 2000, **2**, 503–507.
35 D. Pan, N. Zhao, Q. Wang, S. Jiang, X. Ji and L. An, *Adv. Mater.*, 2005, **17**, 1991–1995.
36 (*a*) W. F. Zhang, M. S. Zhang, Z. Yin and Q. Chen, *Appl. Phys. B*, 2000, **70**, 261–265; (*b*) H. Tang, H. Berger, P. E. Schmid, F. Lévy and G. Burri, *Solid State Commun.*, 1993, **87**, 847–850; (*c*) Y. Lei, L. D. Zhang, G. W. Meng, G. H. Li, X. Y. Zhang, C. H. Liang, W. Chen and S. X. Wang, *Appl. Phys. Lett.*, 2001, **78**, 1125–1127.
37 N. Serpone, D. Lawless and R. Khairutdinov, *J. Phys. Chem.*, 1995, **99**, 16646–16654.